

1 Sill-controlled salinity contrasts followed post-Messinian 2 flooding of the Mediterranean

3 Udara Amarathunga^{1,*}, Andrew McC. Hogg¹, Eelco J. Rohling^{1,2}, Andrew P. Roberts¹, Katharine
4 M. Grant¹, David Heslop¹, Pengxiang Hu¹, Diederik Liebrand^{3†}, Thomas Westerhold³, Xiang
5 Zhao¹, Stewart Gilmore⁴.

6 ¹ Research School of Earth Sciences, Australian National University, ACT 2601, Canberra, Australia

7 ² Ocean and Earth Science, University of Southampton, National Oceanography Centre, Southampton
8 SO14 3ZH, UK

9 ³ MARUM, University of Bremen, D-28359 Bremen, Germany

10 ⁴ Geoscience Australia, GPO Box 378, ACT 2609, Canberra, Australia

11 † Now at PalaeoClimate.Science, Allerton Bywater, United Kingdom

12 * Correspondence to: udara.amarathunga@anu.edu.au

13

14 **5.33 million years ago, a mile-high marine cascade terminated the Messinian Salinity Crisis**
15 **due to partial collapse of the Gibraltar sill that had isolated a largely desiccated**
16 **Mediterranean from the Atlantic Ocean. Atlantic waters may have refilled the basin within**
17 **2 years. Prevailing hypotheses suggest that normal marine conditions were established**
18 **across the Mediterranean immediately after the catastrophic flooding. Here we use proxy**
19 **data and fluid physics-based modelling to show that normal conditions were likely for the**
20 **western Mediterranean (wMed), but that flooding caused a massive transfer of salt from**
21 **the wMed to the eastern Mediterranean (eMed) across the Sicily sill, which became a hyper-**
22 **salinity-stratified basin. Hyper-stratification inhibited deep-water ventilation, causing**
23 **anomalously long-lasting organic-rich (sapropel) sediment deposition. Model-data**
24 **agreement indicates that hyper-stratification breakdown by diapycnal diffusion required**
25 **26,000 years. An alternative hypothesis that Atlantic reconnection occurred after the**
26 **Mediterranean had largely been refilled is inconsistent with our observations, as this would**
27 **have led to hyper-stratification and sapropel formation in both basins. Our findings offer**
28 **insight into the role of stratification in delaying the re-establishment of normal marine**
29 **conditions following abrupt refilling of a previously desiccated ocean basin.**

30 The 630,000-year Messinian Salinity Crisis (MSC) resulted from progressive closure of the
31 connection(s) between the Mediterranean Sea and Atlantic Ocean ~5.96 Million years ago
32 (Ma)^{1–3}. During the MSC, massive evaporite sequences were deposited. A phase of km-scale

33 Mediterranean drawdown occurred⁴, resulting in a basin-wide Messinian erosional surface⁵
34 and 2,500 m and 1,300 m deep Messinian canyons excavated beneath the Nile delta and the
35 Rhône River mouth, respectively^{6,7}. It has long been inferred that Mediterranean sea levels
36 were low, ~1,300 m to ~2,700 m below global sea level^{5,8-11}, prior to the earliest Pliocene
37 (Zanclean) megaflood event that terminated the MSC. Alternatively, geochemical and
38 paleobiological evidence from latest Messinian evaporites may imply elevated basin levels,
39 attributing the drawdown to an older Messinian phase¹². In that scenario, increased
40 Paratethyan and occasional Atlantic inflows are suggested to have largely refilled the
41 Mediterranean¹³ (a shallow Mediterranean base level below Atlantic, with interconnected
42 subbasins) with lower-salinity water overlying deep hypersaline fluids prior to complete
43 Atlantic reconnection¹²⁻¹⁴. We investigate the consequences of abrupt refilling of a partially
44 desiccated basin (a kilometer-scale drawdown in the megaflood hypothesis) and address the
45 alternative hypothesis in a sensitivity test (see Methods, Extended Data Figs. 6-8).

46 **Evidence supporting the megaflood hypothesis**

47 The megaflood hypothesis is based on seismic and borehole data from both the wMed and
48 eMed¹⁵⁻¹⁷. Critical evidence at the Strait of Gibraltar comes from a massive erosive channel
49 in the Gibraltar arc/sill, which extends 390 km from the Gulf of Cadiz on the Atlantic side
50 toward the deep Alboran Sea on the Mediterranean side; the so-called Zanclean channel³.
51 Elongated megabar deposits detected alongside the main erosive channel in the eastern
52 Alboran Sea have been related to the flooding event¹⁶. This sharply defined channel has
53 maximum depth and width of 650 m and 15 km, respectively^{3,16}. The dimensions of this
54 incision have led to model estimates of water fluxes of up to ~150 Sv (Sverdrup, $1 \times 10^6 \text{ m}^3\text{s}^{-1}$)
55 during the Zanclean flood³.

56 The most plausible flood-water passage from the wMed into the eMed is the Noto Canyon,
57 which was carved into the Malta escarpment^{15,16}. Upslope, this canyon comprises a 400 m
58 deep and 4 km wide erosive channel, with Pliocene-Quaternary sediment infill¹⁵. At the Noto
59 Canyon outlet, seismic stratigraphy in the western Ionian basin reveals a buried chaotic
60 sediment body that extends over an 11,000 km² area, and reaches a 1,430–1,620 km³
61 volume^{15,16}. This unit has been interpreted as a megaflood deposit of material that was
62 eroded, transported, and deposited during a catastrophic flooding event at the
63 Miocene/Pliocene transition^{15,16}.

64 The Miocene/Pliocene boundary was drilled at several Deep Sea Drilling Project (DSDP) and
65 Ocean Drilling Program (ODP) sites in the deep Mediterranean¹⁸. It is characterized by a sharp
66 lithological change, which has been attributed to an abrupt return to open-marine conditions
67 across the Mediterranean, terminating the MSC^{16,18,19}. However, where continuous records
68 across the boundary are available, a major difference can be seen between Mediterranean
69 sub-basins (Supplementary Table 1, Extended Data Fig. 1). In the wMed, complete records
70 across the M/P transition from the Tyrrhenian Sea, Balearic margin, and Alboran Sea
71 (Supplementary Table 1) reveal earliest Pliocene foraminifer-nannofossil oozes over Late
72 Messinian evaporative sequences. This sequence suggests that normal marine conditions
73 were established rapidly in the wMed following flooding (Supplementary Table 1). In contrast,
74 eMed cores indicate deposition of a thick organic-rich layer (sapropel) in the earliest Pliocene,
75 which was first detected in DSDP Site 376 from the Florence Rise and named the “mystery
76 sapropel”²⁰. ODP Site 969 on the Mediterranean Ridge contains a similarly thick, laminated
77 sapropel immediately above the flooding surface (Supplementary Table 1). Absence of
78 benthic foraminifera in this sapropel indicates a lack of eMed deep-water ventilation/
79 oxygenation in the immediate flood aftermath, in contrast to better wMed ventilation²⁰.

80 **More evidence for the mystery sapropel**

81 At eMed ODP Site 967 (Eratosthenes seamount), late Messinian brecciated carbonates (with
82 gypsum²¹) are overlain by dark grey to olive green earliest Pliocene sediments^{21,22}.
83 Throughout the sediments younger than ~3.2 Ma at Site 967, colour reflectance records and
84 oxygen isotope stratigraphy indicate a regular pattern of sapropel occurrence, visibly
85 recognizable as dark layers^{21,23,24}. Between 3.2 Ma and 5.33 Ma, there are no visible sapropels,
86 but there are red intervals resulting from post-depositional sapropel oxidation^{21,23,24}
87 (Extended Data Fig.2). These red intervals contain similar Ba enrichments as sapropels, which
88 are associated with organic matter burial and remained present even after post-depositional
89 oxygenation^{25,26}; thus, Ba enrichment is a reliable proxy for original sapropel extents, and for
90 detecting sapropels that were initially present but that were later oxidized^{25–28}. Throughout
91 the last ~14 Myr, sapropel deposition (and associated Ba peaks) consistently occurred during
92 high-amplitude precession-driven insolation maxima, where the amplitude is modulated by
93 orbital eccentricity maxima^{29,30}.

94 Here we present core-scanning X-ray fluorescence (XRF) and magnetic data across the M/P
95 boundary at ODP Site 967 (Supplementary Information) that corroborate the deposition of an
96 organic-rich layer immediately following the M/P transition (Figure 1). From our results, this
97 layer comprises two Ba peaks with lower (but still substantially elevated) Ba levels in between
98 (Figure 1). This Ba pattern is mirrored by two Ti/Al minima with an intervening maximum
99 (Figure 1). In the eMed sapropel stratigraphy, these mirrored fluctuations are typical of two
100 insolation maxima with an intervening minimum^{31–33}. Our chronology suggests that this
101 organic-rich sediment deposition persisted over a 26,000 year period (Extended Data Fig. 3,
102 Supplementary Table 2). Profiles of redox-sensitive elements and anhysteretic remanent
103 magnetization (ARM) across the organic-rich layer (Figure 1) are also typical of
104 sapropels^{25,26,28}. This 26,000-year interval represents the only Neogene example of a sapropel
105 that extends through an insolation minimum; it breaks the well-understood relationship
106 between sapropel deposition and African monsoon maxima associated with northern
107 hemisphere insolation maxima^{29,34–37}. In this conventional mode, monsoon maxima caused
108 extensive freshwater flooding into the Mediterranean^{36,38–40}, which drove both enhanced
109 stratification (curtailing new deep-water ventilation/oxygenation) and enhanced organic
110 export production^{29,41,42}. Meanwhile, the monsoon maximum suppressed wind transport of
111 Ti-rich dust to the eMed^{26,31,43}. Extension of the sapropel at the M/P boundary across an
112 African monsoon minimum (insolation minimum) is a clear indication of the operation of an
113 additional mechanism that was unique to this event with respect to the entire Neogene.

114 **Establishment of normal marine conditions**

115 The terminal Messinian was a period of surface dilution that resulted from increased
116 Paratethyan and riverine freshwater input (*Lago Mare* events), punctuated by local gypsum
117 deposition during times of enhanced evaporation^{32,44,45}. In our main scenario, deep
118 Mediterranean basins prior to the Zanclean flooding were filled with residual high-salinity
119 brines that in places exceeded 2 km in thickness^{9,32,44}. Here, we consider ‘Late Messinian
120 brines’ to have been derived from MSC Stage 2 fluid dilution (when halite precipitated in the
121 wMed and eMed⁴⁵), including potential contributions from halite re-dissolution. We set the
122 brine concentration to 140 PSU (see Methods for explanation on choice of brine salinity). A
123 qualitative conceptual refill scenario can then be formulated based on energy- and mass-
124 balance arguments (the alternative hypothesis starting with a largely refilled late-Messinian

125 basin¹²⁻¹⁴ is addressed in a sensitivity test; see Methods). In the main scenario, the high-
126 energy Atlantic floodwater cascading into a partially desiccated Mediterranean would have
127 encountered and vigorously mixed with residual wMed brines, while the wMed filled to the
128 height of the sill in the Strait of Sicily (Extended Data Fig. 4). Mixed wMed brine would then
129 have broken through and cut the Noto Canyon, cascading into the eMed. Meanwhile, wMed
130 sea level would have remained several hundred metres below Atlantic sea level, which
131 continued the Atlantic cascade through the Zanclean channel, mixing with wMed brines. Thus,
132 we expect massive salt transfer from the steadily diluting wMed into the filling eMed. Once
133 eMed and wMed sea levels equalized, the level across both basins would have risen in unison,
134 until it equalized with Atlantic sea level across the Strait of Gibraltar. Approximately balanced
135 Atlantic inflow and Mediterranean outflow then drove gradual excess salt removal from the
136 Mediterranean. At this stage, stratification was much less pronounced in the wMed than in
137 the eMed because of the prior wMed salt transfer into the eMed (as the latter filled).
138 Inhibition of deep-water ventilation during this hyper-stratified brine-filled eMed period—
139 accentuated by monsoon flooding during insolation maxima—may then explain the
140 anomalously long duration of the “mystery sapropel” spanning two insolation maxima and an
141 intervening minimum.

142 Our qualitative concept requires quantitative assessment, especially to evaluate whether the
143 hypothesized mixing processes are realistic energetically and whether (and why) eMed
144 stratification persisted for ~26,000 years, as derived from our XRF-based sapropel
145 stratigraphy and insolation tuning (see Methods, Extended Data Fig. 3). For this purpose, we
146 present a brine evolution model for the flooding event and its aftermath. Our model considers
147 post-Messinian Mediterranean basin evolution in two successive phases: (i) the Flooding
148 Phase and (ii) an Evolving Phase. The switch between phases occurred when Mediterranean
149 sea level matched Atlantic sea level across the Strait of Gibraltar.

150 The flooding phase is characterized by release of enormous gravitational potential energy.
151 This potential energy is converted to kinetic energy as Atlantic floodwaters cascade into the
152 wMed, which we estimate may have exceeded 1.6×10^{19} J per day at peak flood
153 (Supplementary Figure 1), or more than 500 times the kinetic energy dissipation at Niagara
154 Falls in one year⁴⁶. This energy is sufficient to mix (most of) the existing wMed brines with
155 Atlantic inflow, forming a deep mixed layer atop potential residual brine (Figure 2, see

156 Methods). As the rising wMed sea level reached the crest of the Sicily Sill, mixed wMed waters
157 started cascading into the eMed via Noto Canyon. Given a smaller channel cross-section in
158 Noto Canyon than in the Zanclean channel, we find that an even more energetic flow entered
159 the eMed than the wMed (Supplementary Figure 1). Note that our method calculates the
160 minimum flow, restricted only by channel dimensions, and that more energy would have been
161 available in reality because of the steep drop in this passage^{15,16}. A massive amount of wMed
162 mixed brine was transferred into the eMed through Noto Canyon because the eMed volume
163 is ~2.5 times greater than the wMed, while—at the same time—Atlantic inflow through the
164 Zanclean channel continued to dilute the wMed mixed layer. We find that >95% of the wMed
165 excess salt ended up in the eMed, as this basin filled (Figure 2). Once eMed sea level reached
166 the Sicily Sill, energy transfer across the sill diminished as the cascade terminated gradually.
167 Later, while both basin levels rose together to the Atlantic level, enhanced mixing occurred
168 only in the vicinity of the Gibraltar Sill, further diluting the western basin (Figure 2, Extended
169 Data Figs. 4, 5).

170 At the flooding phase conclusion, dense (post-flood) brines had filled the eMed to the Sicily
171 Sill. For the Mediterranean to return to normal marine conditions, the salt in this brine must
172 have been transferred out of the basin, into the Atlantic Ocean. Eroding the deep brine layer
173 required mixing across the interface separating the brine from shallower, inflow-dominated
174 lower salinity waters. This mixing would have been governed by similar processes to those
175 operating in the modern global ocean: diapycnal mixing due to wind forcing, tidal interaction
176 with bathymetry, and internal wave breaking⁴⁷. These processes lead to estimated diapycnal
177 diffusivity values within a $1-5 \times 10^{-5} \text{ m}^2\text{s}^{-1}$ range⁴⁸; we use this range to estimate mixing
178 timescales and their uncertainties. The wide uncertainty range used here is derived from the
179 competing effects of mixing inhibition owing to stronger stratification and enhanced mixing
180 within a smaller basin (with greater boundary interactions).

181 We model the evolving phase using diapycnal diffusivity in the stated range to remove salt by
182 mixing. We obtain timescales of 10,000-40,000 years (Figure 3b). The ~26,000-year duration
183 estimated from our proxy data agrees well with this range and corresponds to a diapycnal
184 diffusivity of $2 \times 10^{-5} \text{ m}^2\text{s}^{-1}$. We calculate that this process would have released more than $7 \times$
185 10^{16} kg of excess salt into the Atlantic Ocean within that time period, via Mediterranean
186 outflow. Eventually, salt removal from the deeper eMed reduced stratification sufficiently to

187 allow winter-cooled surface waters to attain densities conducive to new deep-water
188 formation. This facilitated restart of deep-water ventilation and oxygenation, which ended
189 the evolving phase marked by the “mystery sapropel.” Downward oxidation of reduced
190 sapropel sediments under an oxygenated water column caused a “burn down” oxidation front
191 in the upper 35 cm of the sapropel^{26–28,49,50} (Figure 1).

192 We propose that absence of a wMed sapropel following the flooding resulted from wMed
193 brine transfer to the eMed during a high-energy mixing and refilling episode. Our sensitivity
194 test evaluates an alternative ending to the MSC, starting with a deep water column of residual
195 brine overlain by lower-salinity brackish waters that had refilled the basin before Atlantic
196 reconnection^{12–14}. We find that there is insufficient energy in this scenario to remove brine
197 from the wMed (Extended Data Figs. 6–8, see Methods), and a long phase of anoxic (sapropel)
198 deposition would be expected in both the wMed and eMed, which conflicts with available
199 observations (Supplementary Table 1). This offers strong support for a partially desiccated
200 Mediterranean state prior to Atlantic reconnection. To account for potential post-Messinian
201 tectonic movements which may have affected the Sicily sill depth^{9,14}, and to test for the
202 minimum wMed and eMed base level drops below Atlantic level required to validate our
203 hypothesis, we perform additional sensitivity tests (Methods). Results of the analysis support
204 available observations, further strengthening our hypothesis (Extended Data Figs. 9, 10).

205 We find that only a kilometer-scale base level fall in both basins at the terminal Messinian
206 would have resulted in the observed proxy records and modelling outcomes. We conclude
207 that the transition from a partially desiccated Mediterranean basin to normal marine
208 conditions was much less rapid than basin refilling; the full transition took ~26,000 years,
209 whereas flooding/refilling took only ~2 years (Figures 2, 3). The ~26,000-year timescale is
210 corroborated quantitatively by our model, which suggests that a 10,000–40,000-year duration
211 is expected. Throughout this time, hyper-stratified eastern Mediterranean conditions caused
212 persistence of an anomalously long interval of organic-rich sediment deposition that
213 extended through two precession-related insolation maxima and the intervening minimum.

214

215

216

Acknowledgements

We thank D. Garcia-Castellanos for providing essential instructions on developing the Mediterranean reflooding model. We also thank P. Meijer for providing the latest Mediterranean hypsometry reconstruction. Study material on fluid dynamics provided by B. Cushman-Roisin encouraged initial model development. This work contributes to Australian Research Council projects FL120100050 and DP2000101157 (EJR), DE190100042 (KMG), DP190100874 (APR), and the Australia-New Zealand IODP Consortium (ANZIC) Legacy/Special Analytical Funding grant LE160100067 (KMG, LRS).

Author contributions

U.A. designed and led the study, and wrote the paper; U.A. developed the hypothesis and performed the modelling, with guidance from A.M.H. and E.J.R.; E.J.R., A.M.H., A.P.R., K.M.G. and D.H. contributed to data interpretation; K.M.G. calibrated scanning XRF data; S.G. performed WD-XRF analyses; X.Z. and P.H. assisted with magnetic measurements; D.L. performed XRF core-scanning; D.L. and T.W. developed the ODP967 composite depth splice; all authors contributed to manuscript development.

Competing interests

The authors declare no competing interests.

218 **Figure 1 | XRF core scanning and magnetic data across the Miocene/Pliocene boundary from ODP**
219 **Site 967.** The Miocene/Pliocene transition is tuned to the 65°N insolation maximum at 5.333 Ma (see
220 Extended Data Fig. 3). Return to normal marine conditions is marked by a sudden jump in Ca
221 concentration at around 5.307 Ma. Elevated Ba concentrations indicate organic matter preservation
222 between the first two Pliocene insolation maxima (Mystery sapropel). The intervening insolation
223 minimum records more than twice as high Ba concentrations compared to normal marine (NM)
224 conditions. (For Ba and Ti/Al, dotted lines in the background indicate original XRF data. Thick lines are
225 the 5-point moving average of the two records). The upper portion of the mystery sapropel has been
226 oxidized as indicated by Mn, S, and ARM profiles (Ox). Me, Messinian; FP, Flooding Phase (Zanclean
227 flooding surface); EP, Evolving Phase.

228 **Figure 2 | Evolution of Mediterranean sub-basins during the Zanclean flood. a,** Sketches of the basin
229 configuration during the latest Messinian (left) and Flooding Phase (right). A = Camarinal Sill; B = Sicily
230 Sill; Z_{wMed}/Z_{eMed} = Messinian drawdown in wMed/eMed; Z_{Sicily} = Depth to Sicily Sill; $Z_{Atlantic}$ = Atlantic Sea
231 surface. **b,** Mixed layer evolution with time for western and eastern basins. Thick black line indicates
232 sea-level rise in both basins with time (wMed and eMed levels). Coloured, hatched, and dotted
233 backgrounds indicate the mixing extent at mixing efficiency (ME) = 0.2, 0.1 and 0.3, respectively. The
234 difference between the basin level curve and the mixed-layer curve gives the mixed layer thickness at
235 a given time. **c,** Reconstructed wMed and eMed hypsometry (left); salinity profile evolution (right) for
236 wMed and eMed at each 100-day interval. Salinity profiles (thick black lines) are given in PSU (from 0
237 to 140 in each diagram). ZFS 1 terminates as the wMed level reaches the Sicily Sill; ZFS 2 terminates
238 as eMed level reaches Sicily Sill; during ZFS 3 both basins rise to the Atlantic level simultaneously. ZFS,
239 Zanclean flood stage; AL, Atlantic Level; SL, Sicily Sill Level; WM, Western Mediterranean; EM, Eastern
240 Mediterranean.

241 **Figure 3 | Mediterranean evolution during the Evolving Phase (EP). a,** A sketch of the main processes
242 involved in brine removal from eMed during the EP. Here, the eMed brine layer formed at the end of
243 the Flooding Phase, as a result of wMed salt transfer and mixing with eMed residual Messinian brines.
244 This layer should not be confused with 'residual Messinian brines' that existed before the flood. **b,**
245 Bottom salinity evolution with time. The thick line is the salinity evolution for diapycnal diffusivity K_S
246 $= 2 \times 10^{-5} \text{m}^2 \text{s}^{-1}$. Upper and lower envelopes mark the evolution at diffusivities of $1 \times 10^{-5} \text{m}^2 \text{s}^{-1}$ and
247 $5 \times 10^{-5} \text{m}^2 \text{s}^{-1}$, respectively. t_{k1} and t_{k5} are the durations taken to erode the brine at $1 \times 10^{-5} \text{m}^2 \text{s}^{-1}$ and
248 $5 \times 10^{-5} \text{m}^2 \text{s}^{-1}$, respectively. The time window between t_{k1} and t_{k5} demarcates all possible time frames
249 within mentioned diffusivity values. t_E is the duration recorded by proxy data (26,000 years). S_{LIW} ,
250 Levantine intermediate water salinity. **c,** Evolution of eMed salinity profile with time for $K_S =$
251 $2 \times 10^{-5} \text{m}^2 \text{s}^{-1}$. Numbers on each curve represent time evolved in thousand years (1 = 1,000 years, etc.)

References

- 252 1. Krijgsman, W., Hilgen, F. J., Raffi, I., Sierro, F. J. & Wilson, D. S. Chronology, causes and
253 progression of the Messinian salinity crisis. *Nature* **400**, 652–655 (1999).
- 254 2. Manzi, V. *et al.* Age refinement of the Messinian salinity crisis onset in the
255 Mediterranean. *Terra Nov.* **25**, 315–322 (2013).
- 256 3. Garcia-Castellanos, D. *et al.* Catastrophic flood of the Mediterranean after the
257 Messinian salinity crisis. *Nature* **462**, 778–781 (2009).
- 258 4. Hsü, K. J., Ryan, W. B. F. & Cita, M. B. Late Miocene Desiccation of the Mediterranean.
259 *Nature* **242**, 240–244 (1973).
- 260 5. Urgeles, R. *et al.* New constraints on the Messinian sealevel drawdown from 3D
261 seismic data of the Ebro Margin, western Mediterranean. *Basin Res.* **23**, 123–145
262 (2011).
- 263 6. Barber, P. M. Messinian subaerial erosion of the proto-Nile Delta. *Mar. Geol.* **44**, 253–
264 272 (1981).
- 265 7. Clauzon, G. Le canyon messinien du Rhone: une preuve decisive du ‘desiccated deep-
266 basin model’ (Hsu, Cita et Ryan 1973). *Bull. Soc. Geol. Fr.* (1982).
267 doi:10.2113/gssgfbull.s7-xxiv.3.597
- 268 8. Gargani, J. & Rigollet, C. Mediterranean Sea level variations during the Messinian
269 salinity crisis. *Geophys. Res. Lett.* **34**, (2007).
- 270 9. Blanc, P. L. Improved modelling of the Messinian Salinity Crisis and conceptual
271 implications. *Palaeogeogr. Palaeoclimatol. Palaeoecol.* **238**, 349–372 (2006).
- 272 10. Meijer, P. T. & Krijgsman, W. A quantitative analysis of the desiccation and re-filling of
273 the Mediterranean during the Messinian Salinity Crisis. *Earth Planet. Sci. Lett.* **240**,
274 510–520 (2005).
- 275 11. Blanc, P. L. The opening of the Plio-Quaternary Gibraltar Strait: Assessing the size of a
276 cataclysm. *Geodin. Acta* **15**, 303–317 (2002).
- 277 12. García-Veigas, J., Cendón, D. I., Gibert, L., Lowenstein, T. K. & Artiaga, D. Geochemical
278 indicators in Western Mediterranean Messinian evaporites: Implications for the
279 salinity crisis. *Mar. Geol.* **403**, 197–214 (2018).
- 280 13. Marzocchi, A., Flecker, R., van Baak, C. G. C., Lunt, D. J. & Krijgsman, W.
281 Mediterranean outflow pump: An alternative mechanism for the Lago-mare and the
282 end of the Messinian Salinity Crisis. *Geology* **44**, 523–526 (2016).
- 283 14. Andreetto, F. *et al.* Freshening of the Mediterranean Salt Giant: controversies and
284 certainties around the terminal (Upper Gypsum and Lago-Mare) phases of the
285 Messinian Salinity Crisis. *Earth-Science Rev.* **216**, 103577 (2021).
- 286 15. Micallef, A. *et al.* Evidence of the Zanclean megaflood in the eastern Mediterranean
287 Basin. *Sci. Rep.* **8**, 1–8 (2018).
- 288 16. Garcia-Castellanos, D. *et al.* The Zanclean megaflood of the Mediterranean –

- 289 Searching for independent evidence. *Earth-Science Rev.* **201**, 103061 (2020).
- 290 17. Camerlenghi, A. *et al.* Seismic markers of the Messinian salinity crisis in the deep
291 Ionian Basin. *Basin Res.* **32**, 716–738 (2020).
- 292 18. Pierre, C., Rouchy, J. M. & Blanc-Valleron, M. M. Sedimentological and stable isotope
293 changes at the Messinian/Pliocene boundary in the Eastern Mediterranean (Holes
294 968A, 969A, and 969B). *Proc. Ocean Drill. Progr. Sci. Results* **160**, 3–8 (1998).
- 295 19. Iaccarino, S. M. & Bossio, A. Paleoenvironment of uppermost Messinian sequences in
296 the Western Mediterranean (site 974, 975, and 978). *Proc. Ocean Drill. Progr. Sci.*
297 *Results* **161**, 529–541 (1999).
- 298 20. Hsu, K. *et al.* Messinian Paleoenvironments. *Initial Reports Deep Sea Drill. Proj. 42 Pt.*
299 *1* 1003–1035 (1978). doi:10.2973/dsdp.proc.42-1.153.1978
- 300 21. Emeis, K. ., Roberston, A. H. . & Richter, C. Site 967, Initial Reports. *Proc. Ocean Drill.*
301 *Progr.* **160**, 215–287 (1996).
- 302 22. Spezzaferri, S., Cita, M. B. & McKenzie, J. A. The Miocene/Pliocene boundary in the
303 eastern Mediterranean: Results from Sites 967 and 969. *Proc. Ocean Drill. Progr. Sci.*
304 *Results* **160**, 9–28 (1998).
- 305 23. Emeis, K. C., Sakamoto, T., Wehausen, R. & Brumsack, H. J. The sapropel record of the
306 eastern Mediterranean Sea - results of Ocean Drilling Program Leg 160. *Palaeogeogr.*
307 *Palaeoclimatol. Palaeoecol.* **158**, 371–395 (2000).
- 308 24. Grant, K. M. *et al.* Organic carbon burial in Mediterranean sapropels intensified
309 during Green Sahara Periods since 3.2 Myr ago. *Commun. Earth Environ.* **3**, 1–9
310 (2022).
- 311 25. Van Santvoort, P. J. M., De Lange, G. J., Langereis, C. G., Dekkers, M. J. & Paterne, M.
312 Geochemical and paleomagnetic evidence for the occurrence of ‘missing’ sapropels in
313 eastern Mediterranean sediments. *Paleoceanography* **12**, 773–786 (1997).
- 314 26. Larrasoña, J. C., Roberts, A. P., Hayes, A., Wehausen, R. & Rohling, E. J. Detecting
315 missing beats in the Mediterranean climate rhythm from magnetic identification of
316 oxidized sapropels (Ocean Drilling Program Leg 160). *Phys. Earth Planet. Inter.* **156**,
317 283–293 (2006).
- 318 27. De Lange, G. J. *et al.* Synchronous basin-wide formation and redox-controlled
319 preservation of a Mediterranean sapropel. *Nat. Geosci.* **1**, 606–610 (2008).
- 320 28. Mercone, D., Thomson, J., Abu-Zied, R. H., Croudace, I. W. & Rohling, E. J. High-
321 resolution geochemical and micropalaeontological profiling of the most recent
322 eastern Mediterranean sapropel. *Mar. Geol.* **177**, 25–44 (2001).
- 323 29. Rohling, E. J., Marino, G. & Grant, K. M. Mediterranean climate and oceanography,
324 and the periodic development of anoxic events (sapropels). *Earth-Science Rev.* **143**,
325 62–97 (2015).
- 326 30. Larrasoña, J. C., Roberts, A. P. & Rohling, E. J. Dynamics of Green Sahara Periods and
327 Their Role in Hominin Evolution. *PLoS One* **8**, (2013).

- 328 31. Wehausen, R. & Brumsack, H. J. Chemical cycles in Pliocene sapropel-bearing and
 329 sapropel- barren eastern Mediterranean sediments. *Palaeogeogr. Palaeoclimatol.*
 330 *Palaeoecol.* **158**, 325–352 (2000).
- 331 32. Ryan, W. B. F. Modeling the magnitude and timing of evaporative drawdown during
 332 the Messinian salinity crisis. *Stratigraphy* **5**, 227–243 (2008).
- 333 33. Lourens, L. J., Wehausen, R. & Brumsack, H. J. Geological constraints on tidal
 334 dissipation and dynamical ellipticity of the Earth over the past three million years.
 335 *Nature* **409**, 1029–1033 (2001).
- 336 34. Hilgen, F. J. Astronomical calibration of Gauss to Matuyama sapropels in the
 337 Mediterranean and implication for the Geomagnetic Polarity Time Scale. *Earth Planet.*
 338 *Sci. Lett.* **104**, 226–244 (1991).
- 339 35. Lourens, L. J. *et al.* Evaluation of the Plio-Pleistocene astronomical timescale.
 340 *Paleoceanography* **11**, 391–413 (1996).
- 341 36. Rossignol-Strick, M., Nesteroff, W., Olive, P. & Vergnaud Grazzini, C. After the deluge:
 342 Mediterranean stagnation and sapropel formation. *Nature* **295**, 105–110 (1982).
- 343 37. Rossignol-Strick, M. African monsoons, an immediate climate response to orbital
 344 insolation. *Nature* **304**, 46–49 (1983).
- 345 38. Osborne, A. H. *et al.* A humid corridor across the Sahara for the migration of early
 346 modern humans out of Africa 120,000 years ago. in *Proceedings of the National*
 347 *Academy of Sciences* **105**, (2008).
- 348 39. Amies, J. D., Rohling, E. J., Grant, K. M., Rodríguez-Sanz, L. & Marino, G. Quantification
 349 of African Monsoon Runoff During Last Interglacial Sapropel S5. *Paleoceanogr.*
 350 *Paleoclimatology* **34**, 1487–1516 (2019).
- 351 40. Rohling, E. J. *et al.* Reconstructing past planktic foraminiferal habitats using stable
 352 isotope data : A case history for Mediterranean sapropel S5. *Mar. Micropaleontol.* **50**,
 353 89–123 (2004).
- 354 41. Rohling, E. J. & Gieskes, W. W. C. Late Quaternary changes in Mediterranean
 355 Intermediate Water density and formation rate. *Paleoceanography* **4**, 531–545
 356 (1989).
- 357 42. Rohling, E. J. Shoaling of the eastern Mediterranean pycnocline due to reduction of
 358 excess evaporation: Implications for sapropel formation. *Paleoceanography* **6**, 747–
 359 753 (1991).
- 360 43. Larrasoaña, J. C. *et al.* Source-to-sink magnetic properties of NE Saharan dust in
 361 Eastern Mediterranean marine sediments: review and paleoenvironmental
 362 implications. *Front. Earth Sci.* **3**, 1–15 (2015).
- 363 44. Rouchy, J. M. & Caruso, A. The Messinian salinity crisis in the Mediterranean basin: A
 364 reassessment of the data and an integrated scenario. *Sediment. Geol.* **188–189**, 35–
 365 67 (2006).
- 366 45. Roveri, M. *et al.* The Messinian Salinity Crisis : Past and future of a great challenge for
 367 marine sciences. *Mar. Geol.* **352**, 25–58 (2014).

- 368 46. Hayakawa, Y. S. & Matsukura, Y. Factors influencing the recession rate of Niagara Falls
369 since the 19th century. *Geomorphology* **110**, 212–216 (2009).
- 370 47. Ferrari, R. & Wunsch, C. Ocean Circulation Kinetic Energy: Reservoirs, Sources, and
371 Sinks. *Annu. Rev. Fluid Mech.* **41**, 253–282 (2009).
- 372 48. Waterhouse, A. F. *et al.* Global Patterns of Diapycnal Mixing from Measurements of
373 the Turbulent Dissipation Rate. *J. Phys. Oceanogr.* **44**, 1854–1872 (2014).
- 374 49. Thomson, J. *et al.* Redistribution and geochemical behaviour of redox-sensitive
375 elements around S1, the most recent eastern Mediterranean sapropel. *Geochim.*
376 *Cosmochim. Acta* **59**, 3487–3501 (1995).
- 377 50. Reitz, A., Thomson, J., Lange, G. J. De & Hensen, C. Source and development of large
378 manganese enrichments above eastern Mediterranean sapropel S1.
379 *Paleoceanography* **21**, 1–17 (2006).

380 **METHODS**

381 **Bulk sediment geochemistry**

382 We present X-ray fluorescence (XRF) core-scanner data from ODP Site 967 for the 5.12-5.35
383 Ma interval. Scanning was performed on archive core-sections at MARUM-University of
384 Bremen on an Avaatech XRF core scanner. Core sections were covered with 4 mm-thick
385 Ultralene film and measured at 50 and 30 kV with 0.55 mA current and with a Cu and Pd-thick
386 filter, respectively, and at 10 kV with 0.035 mA current (no filter); count time for all runs was
387 7 s. Element 'counts' for the entire interval were converted into element concentrations by
388 multivariate log-ratio calibration⁵¹, using new wavelength dispersive (WD)-XRF reference
389 element concentrations. For these, 38 bulk sediment samples were chosen to cover a range
390 of lithologies based on the XRF scan, then 1 cm³ dried ground sample was mixed with a lithium
391 tetraborate/lithium metaborate flux and fused into 39 mm diameter beads. Major element
392 abundances were analysed by WD-XRF using a Bruker S8 Tiger™ spectrometer at Geoscience
393 Australia. Loss on ignition (LOI) was measured by gravimetry after combustion at 1000 °C. One
394 in every ten samples was duplicated along with multiple analyses of 3 international standards
395 (NCS DC70306, MAG-1, ML-2) and an internal basalt standard (WG1). Quantification limits for
396 all major element oxides are <0.2% and reproducibility is within 1%.

397 **Anhyseretic remanent magnetization (ARM)**

398 ODP967 U-channel samples were sliced at 1-cm intervals into discrete non-magnetic 2×2×2
399 cm plastic cubes and measured for ARM on a 2-G Enterprises cryogenic magnetometer at the
400 Australian National University. The ARM was imparted using an alternating field of 100 mT
401 and a direct current bias field of 0.05 mT.

402 **Mediterranean evolution**

403 Evaporative Mediterranean drawdown during the Messinian left residual brines in the
404 adjacent eMed and wMed basins, with thicknesses reaching more than 2 km in the deepest
405 parts^{9,32,44}. We assume a water level drop of 2,000 m below Atlantic sea level in the eastern
406 basin, and 1,750 m in the western basin prior to the megaflood^{5,8-10}. To relate Mediterranean
407 refilling to the volume flux of the incoming flood, we use an intermediate reconstruction
408 between Miocene and present-day Mediterranean hypsometry¹⁰. Before the flood, halite

409 precipitation occurred at ~5.6 Ma in both basins at the Messinian Salinity Crisis (MSC) peak.
 410 The final MSC stage contains gypsum deposition punctuated by surface-water freshening
 411 events. A few drilling sites record gypsum below the flooding surface (Supplementary Table
 412 1). Considering these observations, we set Messinian residual brine salinity to gypsum
 413 saturation at the start of the flood (140 PSU⁵²). We test model outputs for a range of starting
 414 salinities (60-240 PSU) in a sensitivity test (Extended Data Figs. 9, 10).

415 **The Flooding Phase**

416 To determine the flood velocity entering the western basin from the Strait of Gibraltar, we
 417 use a flood incision model, following Garcia-Castellanos et al. (2009)³. This model computes
 418 the incision rate (dz_s/dt) at Camarinal Sill based on the following approach, where dt is the
 419 timestep and dz_s is the depth of erosion per time step:

$$420 \quad \frac{dz_s}{dt} = k_b(\tau_b)^a, \quad (1)$$

421 where k_b and $a = 1.5$ are positive constants. To obtain a final sill incision depth (240 m^{ref. 3}),
 422 we calibrate k_b to $1.8 \times 10^{-4} \text{ m yr}^{-1} \text{ Pa}^{-a}$, where a is the constant mentioned above, while τ_b is
 423 the basal shear stress at the sill, which is computed using:

$$424 \quad \tau_b = \rho_s g (z_s - z_0) S, \quad (2)$$

425 where ρ_s is seawater density, $(z_s - z_0)$ is the mean water depth at the sill, g is acceleration due
 426 to gravity, and $S = z_h/L$ is the ratio between head loss (z_h) and length of the erosive channel
 427 (L). Manning's formula³ is used to calculate the flow velocity:

$$428 \quad v = \frac{1}{n} R_h^{\frac{2}{3}} S^{\frac{1}{2}}, \quad (3)$$

429 where v is the average flow velocity along the slope toward the Alboran basin, $n = 0.05$ is the
 430 roughness coefficient³ and R_h is the hydraulic radius of the passage between the Atlantic and
 431 Mediterranean³. Where channel width is substantially greater than the water depth, the
 432 hydraulic radius is approximated by $(z_s - z_0)$. Flood discharge flux into the Mediterranean (Q) is
 433 then calculated using:

$$434 \quad Q = W(z_s - z_0)v, \quad (4)$$

435 where $W = k_w Q^{a_w}$ is the incision channel width, which increases to a final 14 km value at
 436 the end of the flood. Here $a_w = 0.5$ is a constant, and we impose $k_w = 1.1$ to obtain the final
 437 channel width (see Methods in Garcia-Castellanos et al. (2009) for details³).

438 This model predicts a peak discharge flux that exceeds 100 Sv at a velocity $> 40 \text{ ms}^{-1}$ at the
 439 Camarinal Sill³. In the initial flood stage, high-energy normal Atlantic seawater inflow
 440 encounters much denser residual wMed brines. The extent of mixing between brine and flood
 441 waters depends on the kinetic energy of the flow that approaches the brine surface. Without
 442 mixing, a seawater layer (ρ_s) would form on top of the denser brine (ρ_b). In contrast, if
 443 complete seawater mixing occurred with the brine, a single intermediate density layer (ρ_m)
 444 would have formed. Mixing due to turbulent erosion of stratification can be accomplished
 445 with a large enough energy to overcome the potential energy, raising denser fluid parcels
 446 while lowering lighter parcels⁵³.

447 If complete mixing occurred in the basin, the centre of gravity of the system must be raised,
 448 resulting in a potential energy gain given by:

$$449 \quad PE_{Final} - PE_{Initial} = PE_{Gain} = \int_0^{H+h} \rho_m g z dz A(z) - \left(\int_H^{H+h} \rho_s g z dz A(z) + \int_0^H \rho_b g z dz A(z) \right), \quad (5)$$

450 where PE_{Gain} represents the energy (per day) required for complete mixing, $A(z)$ is the basin
 451 surface area with depth (z), h is the thickness of the seawater layer flooded into the basin per
 452 timestep (per day), and H is the total brine column thickness prior to mixing.

453

454 Under the assumption of the Garcia-Castellanos et al. (2009)³ model that the slope of Atlantic
 455 water inflow into the wMed is constant over time, the flow velocity entering the brine surface
 456 in the western basin, v_{wMed} is v . The kinetic energy per day of this inflow (KE_{wMed}) is then
 457 calculated using:

$$458 \quad KE_{wMed} = \frac{1}{2} \rho_s v_{wMed}^2 Q. \quad (6)$$

459

460 In our model, we calculate energy conversions at daily iterations, by integrating the energy
 461 expression in equation 6 over one-day intervals. Available potential energy of inflow into the
 462 wMed (at the sill), APE_{wMed} , is equal to $\rho_s g Q L_{wMed}$, where L_{wMed} is the vertical distance
 463 between the brine surface and the Camarinal Sill crest. As the Atlantic inflow descended

464 down-slope, gravitational potential energy was released to kinetic energy, and was lost in
 465 processes such as Zanclean channel erosion and turbulent dissipation. Erosion along the slope
 466 will have resulted in a headward-migrating erosion wave along the channel that may have
 467 then triggered even higher flow and erosion rates, resulting in a more abrupt flood⁵⁴.
 468 Therefore, our calculations offer a minimum estimate of flow kinetic energy into the wMed.

469

470 Most of the inflow kinetic energy into the basin is lost to viscous turbulent dissipation.
 471 Laboratory experiments in stratified fluids suggest that ~20% of the turbulent energy loss goes
 472 to irreversibly mixing the stratification (known as the mixing efficiency)^{55,56}. Thus, the energy
 473 available for basin mixing (KE_{Av}) can be given as:

$$474 \quad KE_{Av} = \Gamma \cdot KE_{wMed}, \quad (7)$$

475 where $\Gamma \approx 0.2$ is the mixing efficiency. Full-depth mixing can occur only if $KE_{Av} > PE_{Gain}$.
 476 If available kinetic energy is less than that required to mix the entire brine column thickness
 477 (H), partial brine mixing will occur. The mixing extent can then be computed using energy
 478 arguments. For this purpose, we introduce a mixing depth (H_{Mix}). Where mixing is incomplete,
 479 equation 1 can be rewritten as:

$$480 \quad KE_{Av} = PE_{GPar} = \int_{H+h-H_{Mix}}^{H+h} \rho_m g z dz A(z) - \left(\int_H^{H+h} \rho_s g z dz A(z) + \int_{H+h-H_{Mix}}^H \rho_b g z dz A(z) \right), \quad (8)$$

481 where PE_{GPar} is the potential energy gain during partial mixing. Hence, if available energy is
 482 insufficient to mix completely, mixing will be restricted to a brine depth of H_{Mix} . If the flow
 483 kinetic energy increases with time, H_{Mix} will increase accordingly, eventually completely
 484 mixing the brine when KE_{Av} exceeds PE_{Gain} .

485 We use the following approach to calculate the salinity evolution (S_m) of the mixed fluid:

$$486 \quad S_m = \frac{Q_{SAW} + Q_b S_b}{Q_m} = S_{wMed}, \quad (9)$$

487 where Q_b is the brine volume (per day) mixed in the basin, S_b is the brine salinity, and Q_m is
 488 the resultant volume of mixed fluid (per day). For salinity-density conversions, we include the
 489 Gibbs Sea Water (GSW) Oceanographic Toolbox functions into our model.

490 Once wMed sea level reaches the Sicily Sill (430 m below sea level), wMed mixed fluid spills
 491 into the eMed. We use equation (8) to compute the mixing extent in the eastern basin as it

492 fills. Noto Canyon is considered to be the path of flood waters into the Ionian basin (eMed)
 493 during the megaflood¹⁵. To approximate the flow velocity approaching the eMed brine
 494 surface, we consider that the volume flux spreads across a channel of width b_{eMed} , in a fluid
 495 layer of depth d_{eMed} travelling at velocity v_{eMed} . The erosive channel detected at the upper
 496 Noto Canyon is 4 km wide; thus, we impose b_{eMed} to be a 4 km maximum. The present average
 497 channel depth is 400 m^{ref 15,16} (d_{eMed}). Minimum flow velocity into the eMed is then given by:

$$498 \quad v_{eMed} = \frac{Q}{A_{Noto}}, \quad (10)$$

499 where A_{Noto} is the present-day maximum cross-sectional area of the Noto Canyon erosive
 500 channel. In reality, flow velocity entering the eMed would have been higher due to the steep
 501 slope toward the end of the passage^{15,16}. The kinetic energy of flow entering the brine is:

$$502 \quad KE_{eMed} = \frac{1}{2} \rho_s (v_{eMed}^2) Q. \quad (11)$$

503

504 Similar to the wMed approach, complete mixing is assumed if $1 > (\Gamma KE_{eMed})/PE_{Gain}$. As the eMed
 505 is filled, wMed waters mix continuously due to inflow through the Strait of Gibraltar. Equation
 506 (9) is used to calculate salinity evolution in both basins during this flood stage (S_{wMed} and S_{eMed} ,
 507 respectively). The water flow cascading into the Ionian basin (eMed) terminates once the
 508 eMed level reaches the Sicily Sill level. Thereafter, both eMed and wMed levels rise
 509 simultaneously to the Atlantic level. In this final flood stage, mixing occurs due to flow along
 510 the Zanclean channel (Strait of Gibraltar), further diluting the western basin (thus, further
 511 decreasing S_{wMed}).

512 **The Evolving Phase**

513 During the first part of our model (*Flooding Phase*), most wMed salt was transferred into the
 514 eMed across the Strait of Sicily. As a result, the wMed had less saline waters, whereas the
 515 eMed filled with a denser brine layer up to the Sicily Sill (the reconstructed early Pliocene
 516 eMed volume with sea level equal to the Sicily Sill level is $2.04 \times 10^{15} \text{ m}^3$ ref. 10). For the
 517 Mediterranean to return to normal marine conditions, this enormous amount of brine should
 518 then have been redirected to the Atlantic Ocean.

519 The processes required to erode this deep, dense brine layer would have involved mixing
 520 across the interface separating it from inflowing waters. This mixing would occur due to the
 521 same set of processes that operate in the modern global ocean; namely, diapycnal mixing due

522 to internal wave breaking^{47,57}. Generation of internal gravity waves results from a chain of
 523 processes including barotropic tidal flow over topography, variations in wind force at the
 524 ocean surface, lee waves produced by ocean currents, and eddies flowing over
 525 topography^{47,57}. The sum of all turbulent processes leads to an effective turbulent diffusivity
 526 of $K_S = 1-5 \times 10^{-5} \text{ m}^2\text{s}^{-1}$ refs. 48,57. By assuming a turbulent diffusivity in this range, we estimate
 527 the duration required to erode the deep layer. The salinity profile immediately after the
 528 flooding event consists of an upper Mediterranean seawater layer, and a deep brine layer
 529 below the sill depth. Mixing and advection is rapid in the x and y directions (horizontally);
 530 thus, a good approximation for salinity, S , at any time is that it depends on height, z , only. The
 531 diffusive timescale, t , can be estimated from the diffusion equation:

$$532 \quad \frac{\partial S}{\partial t} = K_S \frac{\partial^2 S}{\partial z^2}. \quad (12)$$

533 To solve Eq. (12) numerically, we divide the domain into N equally spaced layers, each having
 534 thickness d_z . Basin hypsometry is characterized by the surface area (A_z) at each depth interval.
 535 The salt flux between adjacent layers is proportional to the local salinity gradient given by:

$$536 \quad F \sim K_S \frac{\partial S}{\partial z}. \quad (13)$$

537 Evolution of salinity in the j^{th} layer of the domain is given by the flux divergence:

$$538 \quad A^j \frac{\partial S^j}{\partial t} = \frac{K_S}{d_z} \left(A^{j+1} \left[\frac{S^{j+1} - S^j}{d_z} \right] - A^j \left[\frac{S^j - S^{j-1}}{d_z} \right] \right). \quad (14)$$

539 When this equation is further discretized in time, it can be shown that:

$$540 \quad S_{\tau+1}^j = S_{\tau-1}^j + \frac{2K_S d_t}{d_z^2} \left(S_{\tau}^{j-1} - \left[\frac{A^{j+1}}{A^j} + 1 \right] S_{\tau}^j + \left[\frac{A^{j+1}}{A^j} \right] S_{\tau}^{j+1} \right), \quad (15)$$

541 where d_t is the time step and time levels are indicated by the subscript (τ). With use of these
 542 equations, we compute the salinity profile evolution until the basin reached modern eMed
 543 salinity values. Diffusive transport of salt from deeper layers to upper eastern basin layers will
 544 be balanced by salt transport to the wMed, and ultimately into the Atlantic Ocean via the
 545 Mediterranean outflow.

546

547 **Sensitivity test Part 1: Basin evolution for a largely refilled Mediterranean (alternative**
548 **hypothesis)**

549 The nature of the MSC termination has long been debated. One hypothesis is a catastrophic
550 termination (the main scenario of this paper) that resulted from Camarinal Sill collapse in the
551 Strait of Gibraltar^{3,11,15,16}. This hypothesis considers a km-scale drawdown of water in
552 Mediterranean sub-basins prior to the reconnection. An alternative hypothesis interprets an
553 almost-filled Mediterranean during the final MSC stage (Lago Mare), which was connected to
554 the Atlantic and/or Paratethys prior to the termination^{12,14,58}.

555 Here we present a sensitivity test to evaluate the validity of our hypothesis (a partially-
556 desiccated Mediterranean leading to catastrophic termination), compared to a scenario
557 where the basin is filled to the Sicily Sill before the termination. We argue that the sapropel
558 presence immediately after the Miocene/Pliocene boundary in eMed cores (Supplementary
559 Table 1) resulted from basin stratification after the Zanclean megaflood. In contrast, no wMed
560 sapropels were found following the M/P boundary. We suggest that absence of a wMed
561 sapropel resulted from brine transfer to the eMed during an abrupt refilling event.

562 If the present-day Black and Caspian Seas were completely emptied into the Mediterranean,
563 this would result in a ~250 m thick layer at the Mediterranean surface¹³. This gives a high-end
564 estimate of Paratethyan inflow to the Mediterranean if the two basins were connected during
565 the Lago Mare phase. It has been suggested that gypsum precipitation resulted from
566 evaporated Paratethyan surface waters (above denser residual brines) at a salinity of ~40
567 PSU⁵⁸. Therefore, we simulate emptying of a volume equivalent to the present-day Black and
568 Caspian Seas into the Mediterranean and allow it to evaporate to a salinity of 40 PSU. If the
569 top of such a layer sits at the crest of the Sicily Sill (430 m), it will be about 130 m in thickness
570 (calculated using a reconstructed Mediterranean hypsometry¹⁰), and will extend below the
571 sill crest to a depth of 560 m.

572 Numerical modelling has shown that halite precipitation during the MSC peak (Stage 2, 5.59-
573 5.55 Ma) resulted from complete disconnection from the Atlantic⁵⁹. Complete isolation will
574 result in basin drawdown due to excess evaporation that will come to equilibrium within a
575 few thousand years (3 to 8 kyr)^{9,10}. The idea of a km-scale drawdown is also supported by the
576 existence of a basin-wide Messinian Erosional Surface (MES)⁵ and deep canyons excavated

577 beneath the Nile delta and Rhône River mouth^{6,7}. Similar to our main scenario, we assume a
 578 wMed deep brine layer at gypsum saturation (140 PSU) below 1750 m, which formed as a
 579 result of MSC stage 2 drawdown. From 560 m to 1750 m, we allow salinity to increase linearly
 580 from 40 to 140 PSU, to obtain a conservative estimate (Extended Data Fig. 6a).

581 Starting with this basin configuration, we compute wMed basin evolution (Extended Data Fig.
 582 6b) during a refilling event resulting from inflow through the Strait of Gibraltar using the
 583 Flooding Phase model. Here we re-calibrate the channel width coefficient (k_w) to allow the
 584 inflow channel to evolve up to the same dimensions as in our main scenario. We then
 585 compare the refilling and basin evolution in both scenarios (Extended Data Fig. 6c). Our
 586 findings suggest that for a filled Mediterranean up to the crest of the Sicily Sill, reconnection
 587 with the Atlantic results in a much longer episode of refilling. The total kinetic energy released
 588 during such a scenario will be >50 times smaller compared to a catastrophic termination,
 589 which is insufficient to erode the deeper brine in the wMed and would result in persistence
 590 of a density-stratified wMed (Extended Data Fig. 6b, c). In that case, we argue that a sapropel
 591 should be expected in the wMed after Atlantic reconnection. Absence of a wMed sapropel
 592 provides strong support for catastrophic MSC termination and for a drawn-down
 593 Mediterranean prior to Atlantic reconnection. We also test this scenario for even lower
 594 salinity profiles between a thin surface layer and deep brines (from 560 m to 1750 m), to
 595 assess if the flood energy was sufficient to erode wMed deep brines, if the mid-layer salinity
 596 was lower (Extended Data Fig. 7a, b). This test run confirms that the energy is insufficient to
 597 remove wMed deep brines even for a 100% mixing efficiency.

598 **Sensitivity test Part 2: Basin evolution at initial salinities < 140 PSU (Main scenario)**

599 In order to test the validity of our hypothesis in case the residual Messinian fluid salinity was
 600 lower than 140 PSU, we computed the salinity evolution of the wMed and eMed using the
 601 same approach in the Flooding Phase used for the main scenario. We use a range of salinities
 602 from 60 to 120 PSU. Then we use the Evolving Phase to determine the duration of brine
 603 removal at different initial salinities (Extended Data Fig. 7c, d). At salinities lower than 140
 604 PSU, all wMed salt is transferred to the eMed, resulting in a salinity approximated by:

$$605 \quad S_{eMed} = \frac{(V_{eMed(Sicily)} - V_{b(eMed)} - V_{b(wMed)}) \times S_{Atl} + (V_{b(eMed)} + V_{b(wMed)}) \times S_b}{V_{eMed(Sicily)}} \quad (16)$$

606 where S_{eMed} is the final eMed salinity below the Sicily Sill, $V_{eMed(Sicily)}$ is the total eMed volume
607 at the Sicily Sill, $V_{b(eMed)}$ and $V_{b(wMed)}$ are the residual Messinian volumes in eMed and wMed,
608 and S_b is the initial Mediterranean fluid salinity. For a range of initial residual Messinian brine
609 salinities from 60 to 120 PSU, we find that the salt removal period varies between ~14,000 to
610 22,000 years.

611 **Sensitivity test Part 3: Basin evolution at initial salinities > 140 PSU (Main scenario)**

612 In order to test the validity of the hypothesis in case the residual Messinian salinities were >
613 140 PSU, we compute the salinity evolution of the wMed and eMed using Flooding Phase
614 calculations for 160-240 PSU. We employ the Evolving Mode approach to estimate salt
615 removal duration for both basins, when excess salt remains at the end of the flooding phase.
616 If wMed stratification was less than the resulting winter water density, convective overturn
617 would mix surface and deep waters, removing the additional salt. In the present-day wMed,
618 surface salinities reach 38.0-38.4 PSU in winter, with reduced temperatures of 10-12 °C^{ref.29}.
619 We assume a constant brine temperature of 20 °C during the flooding phase. Therefore, we
620 calculate the sea water salinity at 20 °C for an equivalent wMed winter surface water density.
621 We use this as a limit in determining the brine removal period in the evolving phase (Extended
622 Data Fig. 8). Results of the sensitivity test indicate that all wMed salt would transfer to the
623 eMed up to initial brine salinities of 170 PSU. From 170 to 200 PSU, final mixed wMed waters
624 have a higher-than-winter water density. Above 220 PSU, residual Messinian brines remain in
625 the deep wMed, implying that flood energy was insufficient to erode the deep brines. Above
626 170 PSU initial salinity, we find that it would take about 4,000 to 12,000 years to remove
627 wMed salt by diffusion. Combining the information from Sensitivity Test Parts 2 and 3, we
628 conclude that our model results agree reasonably with the data for starting salinities across
629 the 60-170 PSU range.

630 **Sensitivity test Part 4: Basin evolution with the change of Sicily sill depth**

631 To test the effect of Sicily sill depth on basin evolution during the flooding mode, we modified
632 our model for shallower and deeper than present Sicily sill depth. For this, we employed ~0.7
633 and ~1.3 times the present sill depth (300 m and 560 m, respectively). We find that the
634 flooding mode length reduces/increases when the Sicily sill depth is shallower/deeper than
635 present. We find that independent of the sill depth, a majority of the wMed Messinian salt is

636 transferred to the eMed across the sill (Extended Data Fig. 9). Our model suggests that as the
637 sill gets shallower, there is slightly more salt remaining in the wMed, compared to the deeper
638 sill setting. Detailed palaeomagnetic studies have shown that the Sicily sill may have been
639 uplifted to its present depth during central to eMed wide middle-late Pliocene tectonic
640 events^{24,60}. Modelling experiments have also suggested a deeper Sicily sill during the
641 Messinian^{9,10,14}. Our model results would agree with these observations, as more wMed salt
642 would be transferred to the eMed for a deeper sill.

643 **Sensitivity test Part 5: Effect of the initial base level on basin evolution**

644 We have assumed initial base levels for the wMed (1,750 m below Atlantic level) and the
645 eMed (2,000 m) for our main scenario, based on available references. In sensitivity test part
646 1 (alternative scenario), we tested basin evolution when the Mediterranean is filled up to the
647 Sicily sill. To test the effect of intermediate base levels, and to define a minimum base level
648 which validates the hypothesis, we computed basin evolution by stepwise increasing the base
649 level in 100 m increments in both basins. For each step of base level increase above the main
650 scenario base levels, we filled both wMed and eMed with lower salinity waters following the
651 steps of sensitivity test part 1. From 1,750 m up to 1,450 m base level in the wMed (2,000 to
652 1,700 m in the eMed), all the residual Messinian salt is transferred from wMed to the eMed.
653 When the base level is increased above this point, excess salt tends to remain in the wMed.
654 We have shown test results up to 1,250 m wMed base level; corresponding to a 1,500 m eMed
655 base level (Extended Data Fig. 10). A period of 2,500 to 4,500 years is required to remove the
656 excess salt by diffusion when the wMed level is above 1,450 m.

Data availability

ODP Site 967 data from this study are available from Pangaea (www.pangaea.de) under 'Scanning XRF and environmental magnetic data across the Miocene-Pliocene boundary from ODP Site 967 (Eastern Mediterranean)' and are also available as online Supplementary Data accompanying this article.

Code availability

All the figures in this manuscript are reproducible via Jupyter notebooks and instructions provided in the Github repository Med_evolution_megaflood⁶¹ (<https://doi.org/10.5281/zenodo.6528768>).

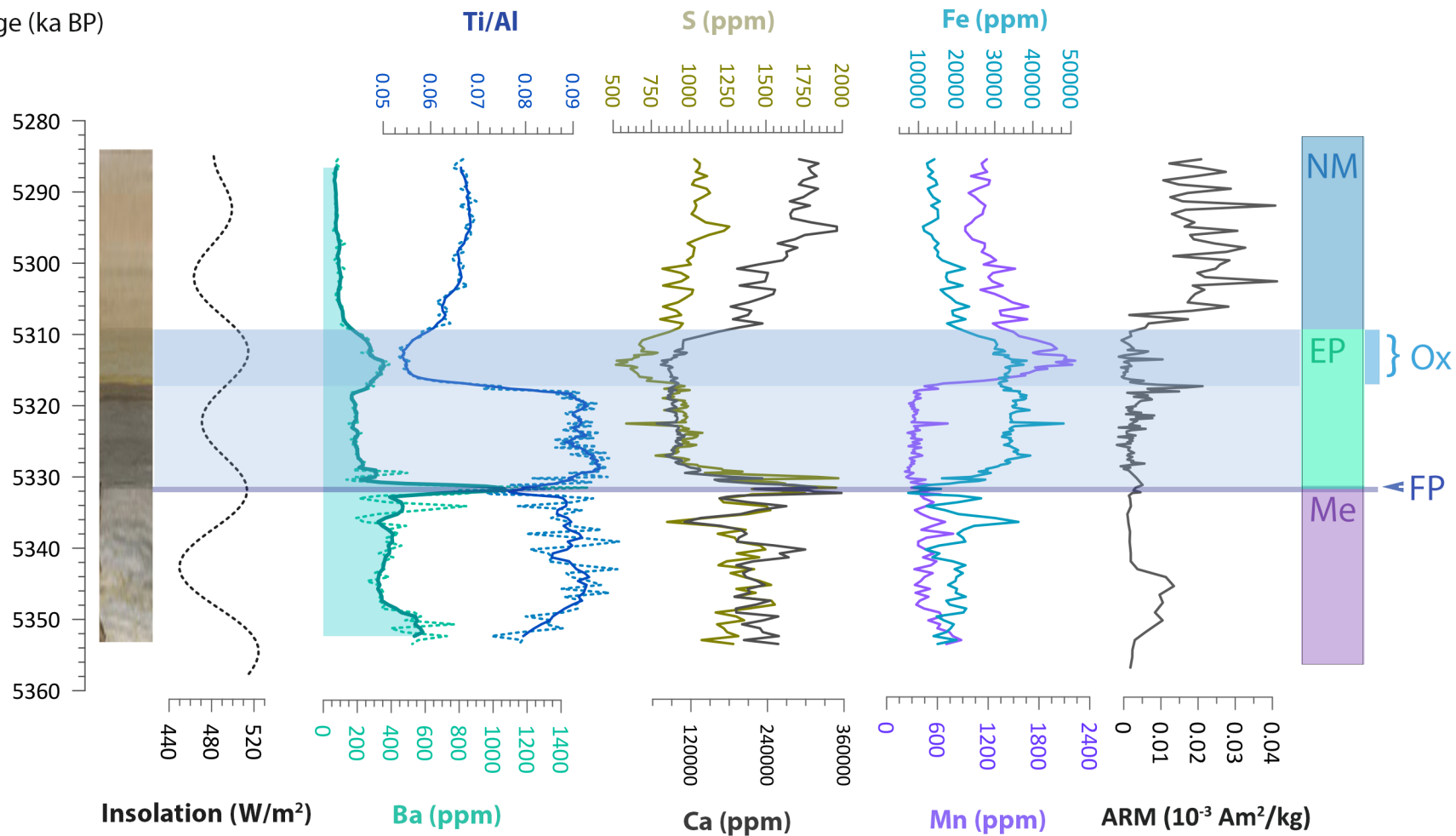
- 657 51. Weltje, G. J. *et al.* Prediction of geochemical composition from XRF core scanner data:
658 A new multivariate approach including automatic selection of calibration samples and
659 quantification of uncertainties. in *Micro-XRF studies of sediment cores* (eds. Croudace,
660 I. W. & Rothwell, R. G.) 507–534 (Springer, 2015). doi:10.1007/978-94-017-9849-5_21
- 661 52. Rohling, E. J., Schiebel, R. & Siddall, M. Controls on Messinian Lower Evaporite cycles
662 in the Mediterranean. *Earth Planet. Sci. Lett.* **275**, 165–171 (2008).
- 663 53. Cushman-Roisin, B. & Beckers, J.-M. *Introduction to Geophysical Fluid Dynamics-*
664 *Physical and Numerical Aspects*. (Academic Press, 2011).
- 665 54. Garcia-Castellanos, D. & O’Connor, J. E. Outburst floods provide erodability estimates
666 consistent with long-term landscape evolution. *Sci. Rep.* **8**, 1–9 (2018).
- 667 55. Peltier, W. R. & Caulfield, C. P. Mixing efficiency in stratified shear flows. *Annu. Rev.*
668 *Fluid Mech.* **35**, 135–167 (2003).
- 669 56. Osborne, T. . Estimates of the Local Rate of Vertical Diffusion from Dissipation
670 Measurements. *J. Phys. Oceanogr.* **10**, 83–89 (1980).
- 671 57. MacKinnon, J. A. *et al.* Climate process team on internal wave-driven ocean mixing.
672 *Bull. Am. Meteorol. Soc.* **98**, 2429–2454 (2017).
- 673 58. Grothe, A. *et al.* Paratethys pacing of the Messinian Salinity Crisis: Low salinity waters
674 contributing to gypsum precipitation? *Earth Planet. Sci. Lett.* **532**, 116029 (2020).
- 675 59. Garcia-Castellanos, D. & Villaseñor, A. Messinian salinity crisis regulated by competing
676 tectonics and erosion at the Gibraltar arc. *Nature* **480**, 359–363 (2011).
- 677 60. Duermeijer, C. E. & Langereis, C. G. Astronomical dating of a tectonic rotation on
678 Sicily and consequences for the timing and extent of a middle Pliocene deformation
679 phase. *Tectonophysics* **298**, 243–258 (1998).
61. Amarathunga, U. & Hogg, A. M. Resurgence of Mediterranean after the Zanclean
megaflood - Jupyter notebooks (Python). (2022). doi:10.5281/zenodo.6528768
62. Grant, K. M. *et al.* A 3 million year index for North African humidity/aridity and the
implication of potential pan-African Humid periods. *Quat. Sci. Rev.* **171**, 100–118
(2017).
63. Laskar, J., Fienga, A., Gastineau, M. & Manche, H. La2010: A new orbital solution for
the long-term motion of the Earth. *Astron. Astrophys.* **89**, 1–15 (2011).

Materials & Correspondence should be addressed to U.A. (udara.amarathunga@anu.edu.au)

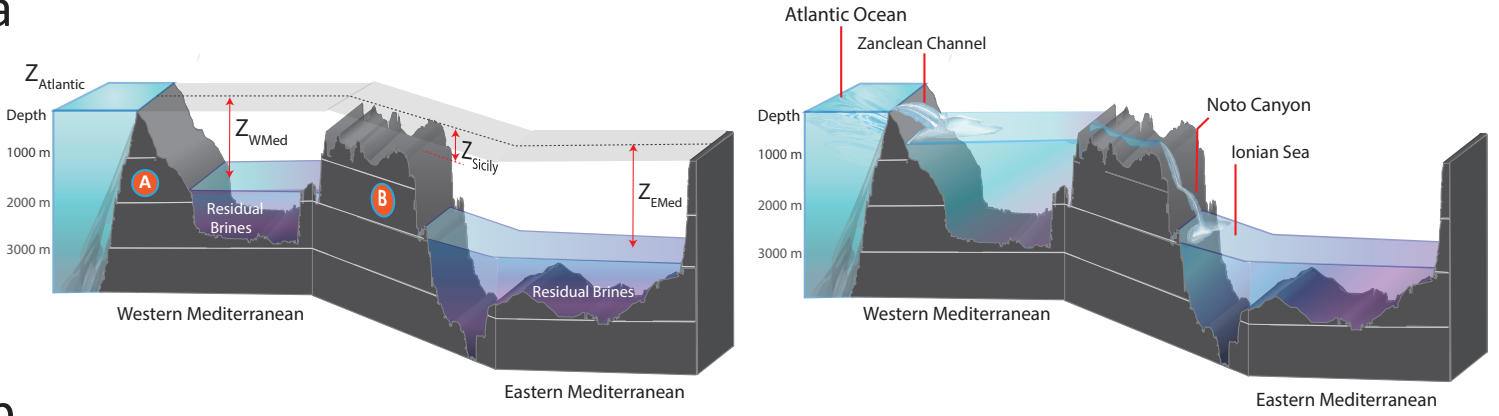
Additional information

Supplementary information is available for this manuscript

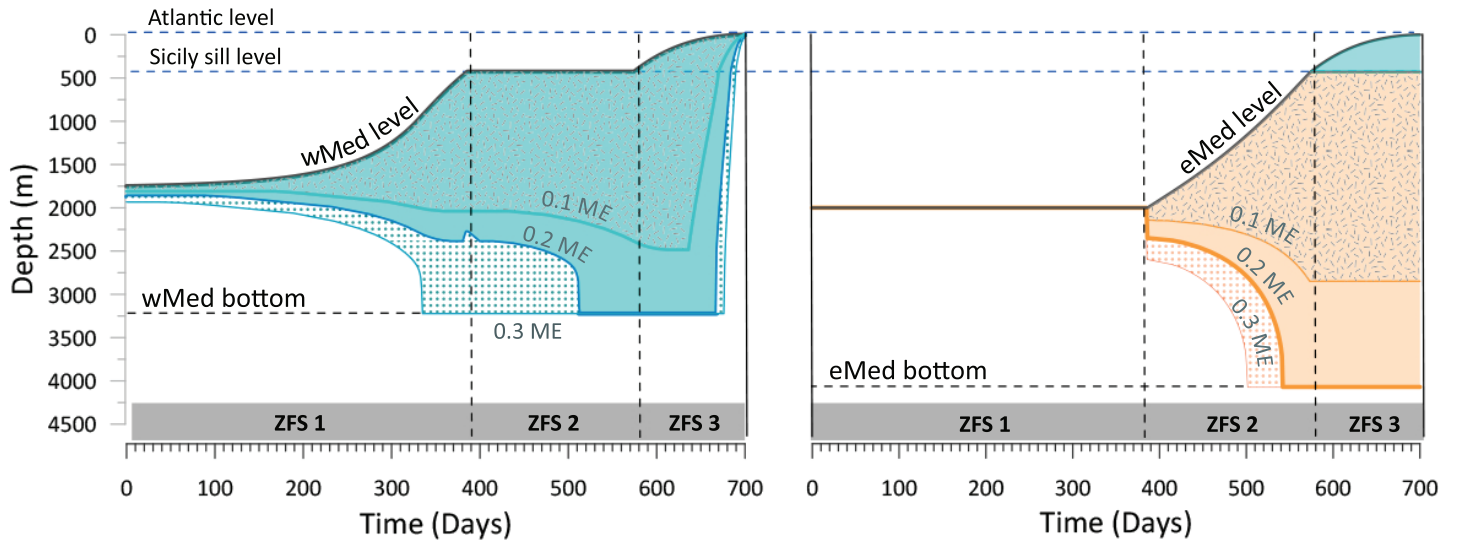
Age (ka BP)



a



b



c

